THz pulse train generation through ultrafast development of surface plasmon-polariton modulation instability

Article *in* Journal of Optics · November 2021

DOI: 10.1088/2040-8986/ac3c4f

CITATIONS
0

READS
15

5 authors, including:

Dmitry A. Korobko
Ulyanovsk State University
139 PUBLICATIONS **548** CITATIONS

SEE PROFILE

Sergey Moiseev
Ulyanovsk State University
90 PUBLICATIONS **406** CITATIONS

SEE PROFILE

Alexey S. Kadochkin
Ulyanovsk State University
59 PUBLICATIONS **206** CITATIONS

SEE PROFILE

IOP Publishing Journal of Optics
J. Opt. **24** (2022) 015002 (8pp) https://doi.org/10.1088/2040-8986/ac3c4f

THz pulse train generation through ultrafast development of surface plasmon-polariton modulation instability

Dmitry A Korobko[1,*], Igor O Zolotovskii[1,2], Sergey G Moiseev[1,2,3], Alexey S Kadochkin[1,2] and Vyacheslav V Svetukhin[4]

[1] Ulyanovsk State University, Ulyanovsk, Russia
[2] Institute of Nanotechnologies of Microelectronics of the Russian Academy of Sciences, Moscow, Russia
[3] Kotelnikov Institute of Radio Engineering and Electronics of the Russian Academy of Sciences, Ulyanovsk Branch, Ulyanovsk, Russia
[4] Scientific-Manufacturing Complex Technological Centre, Moscow, Russia

E-mail: korobkotam@rambler.ru

Received 22 September 2021, revised 3 November 2021
Accepted for publication 22 November 2021
Published 14 December 2021

Abstract

Propagation of high-intensity electromagnetic waves in a waveguide structure could initiate nonlinear effects resulting in drastic changes of their spatial and temporal characteristics. We study the modulation instability effect induced by propagation of surface plasmon polaritons in a silver thin-film waveguide. The nonlinear Schrodinger equation for propagating surface plasmon wave is obtained. It is shown numerically that the modulation instability effect can give rise to ultrafast spatial redistribution and longitudinal localization of surface plasmon-polariton wave energy in subwavelength scale. The dependence of plasmon wave dispersion and nonlinear characteristics on metal film thickness is considered. We demonstrate that the use of films with the thickness varying along the waveguide length allows reduction of the generated pulse width and increase of frequency comb bandwidth. The proposed technique is promising for design of ultra-compact (tens of nm) optical generators delivering pulse trains with the repetition rate higher than 1 THz.

Keywords: plasmon-polaritons, modulation instability, high repetition rate pulse trains

(Some figures may appear in color only in the online journal)

1. Introduction

The use of surface plasmon polaritons (SPP) allows breaking out the conventional diffraction limit to design ultra-compact optical components comparable with electronic components on a crystal [1, 2]. A strong confinement of SPP enables integration of advanced photonics with electronic components on a submicron scale, thereby opening prospects for elaboration of ultra-fast energy-efficient tools for high-speed data processing [3, 4]. Recently proposed [5, 6] effective methods of ohmic loss compensation for SPP propagating in plasmonic waveguides have opened the way for new applications of SPP in the integrated nanophotonic circuits. The transition from optical to plasmonic format could bring a breakthrough in tackling modern technological problems. In this context, we propose to utilize the specific nonlinear and dispersion properties of SPP to get a drastic increase of the pulse repetition rate ($\geqslant$1 THz) available with the master oscillators based on integrated micro (nano) circuits. The proposed concept is very promising for generation of clock frequencies in high-performance computers. Therefore, the present study is focused on the development of a plasmonic structure employed as a generator of

* Author to whom any correspondence should be addressed.

ultrashort pulses with a clock frequency >1 THz that is a key element in optical computing systems.

Modulation instability (MI), a fundamental effect provoking an explosive growth of weak perturbations in a nonlinear physical system [7], underlies the operation of the high repetition rate optical pulse generator. In optics, the MI can be employed for transformation of continuous weakly modulated wave into a pulse train. Propagation of the modulated wave in an optical waveguide [8] is one of the most illustrative cases of MI developed in the systems described by the nonlinear Schrödinger equation (NLS). Also, similar processes could be observed in optical cavities [9], spatial-time dynamics of laser beams [10], during the formation of stable optical structures in waveguides, etc [11]. Commonly, MI is considered as a parasitic effect causing an increase of noise disturbances and limiting the parameters of coherent signal transmission lines [12]. However, MI is highly promising in some applications, such as generation of high repetition rate short pulse trains [13, 14]. Superposition of two monochromatic optical waves operating different wavelengths is commonly used as the pump signal to generate a train of short optical pulses in the single-mode optical fiber through the MI [15]. In this work, we apply this technique to generate a high repetition rate pulse train through evolution of a continuous strongly confined SPP. To the best of our knowledge, for the first time, we explore the effect of film thickness on the MI generation process and consider the use of metal films with varying thickness for generation of ultrashort pulse trains with a high repetition rate through the MI.

2. Nonlinear equation for SPP

Let us consider a quasi-monochromatic SPP wave propagating with the carrier frequency ω_0 and propagation constant β_0 in a structure with the conductive film surrounded by two dielectric half spaces (figure 1). Taking into account the dependence of the medium dielectric permittivity (DP) on the radiation intensity I, the function $\beta = \beta(I,\omega)$ can be expanded in the Taylor series in the vicinity of point $\omega = \omega_0$, $I = 0$:

$$\beta \approx \beta_0 + (\omega-\omega_0)\left.\frac{\partial\beta}{\partial\omega}\right|_{\omega_0,I=0} + \frac{1}{2}(\omega-\omega_0)^2\left.\frac{\partial^2\beta}{\partial\omega^2}\right|_{\omega_0,I=0} + \\ + \frac{1}{6}(\omega-\omega_0)^3\left.\frac{\partial^3\beta}{\partial\omega^3}\right|_{\omega_0,I=0} + I\left.\frac{\partial\beta}{\partial I}\right|_{\omega_0,I=0}. \quad (1)$$

Using:

$$\Omega = \omega-\omega_0,\ K = \beta-\beta_0,$$

expression (1) reduces to a nonlinear dispersion relation:

$$K = \beta_1\Omega + \frac{1}{2}\beta_2\Omega^2 + \frac{1}{6}\beta_3\Omega^3 + \gamma I, \quad (2)$$

where:

$$\beta_1 = \left.\frac{\partial\beta}{\partial\omega}\right|_{\omega_0,I=0}, \quad (3)$$

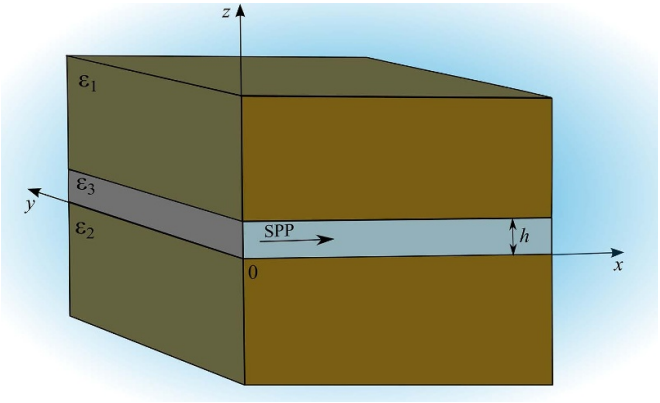

Figure 1. Structure with the conductive film of thickness h surrounded by two dielectric half spaces with the DPs ε_1 and ε_2.

is the parameter determined by the group velocity:

$$v_g = \left.\frac{\partial\omega}{\partial\mathrm{Re}[\beta]}\right|_{\omega_0,I=0}, \quad (4)$$

$$\beta_2 = \left.\frac{\partial^2\beta}{\partial\omega^2}\right|_{\omega_0,I=0} \quad (5)$$

is the group velocity dispersion (GVD),

$$\beta_3 = \left.\frac{\partial^3\beta}{\partial\omega^3}\right|_{\omega_0,I=0} \quad (6)$$

is the third-order dispersion (TOD),

$$\gamma = \left.\frac{\partial\beta}{\partial I}\right|_{\omega_0,I=0} = \beta_1\left.\frac{\partial\omega}{\partial I}\right|_{\omega_0,I=0} \quad (7)$$

is the parameter of Kerr nonlinearity at $\omega = \omega_0$.

In the approximation of slowly varying amplitudes, the quasi-monochromatic SPP wave field can be expressed as $A(x,t)U(y,z)\exp[i(\beta_0 x-\omega_0 t)]$, where $A(x,t)$ is a function slowly varying in time, the parameters β_0 and ω_0 are the real values. Oscillation periods of the wave packet envelope $A(x,t)$ in time and space (coordinate x) are determined by Ω and K, $U(y,z)$ is the transverse wave field profile in a thin-film plasmon waveguide. Since the relations:

$$\frac{\partial A}{\partial t} \approx -i\Omega A,\ \frac{\partial A}{\partial x} \approx iKA,$$

are true for the wave packet envelope, dispersion relation (2) can be associated with the NLS equation describing the dynamics of SPP wave complex amplitude:

$$\frac{\partial A}{\partial x} + \beta_1\frac{\partial A}{\partial t} + \frac{1}{2}i\beta_2\frac{\partial^2 A}{\partial t^2} - \frac{1}{6}\beta_3\frac{\partial^3 A}{\partial t^3} - i\gamma|A|^2A = 0, \quad (8)$$

where $|A|^2 = I$ is the wave intensity. In particular, equation (8) describes the rapid growth of weak time-periodic perturbations of the steady-state solution, an effect of MI [8]. In the next section, the structure parameters at which MI is implemented for SPP within the visible spectrum range will be defined.

3. SPP wave dispersion parameters in conductive film of constant thickness

Let us consider a layered structure (figure 1) comprising two semi-infinite media separated by a thin conductive film of constant thickness h. The real part ($\mathrm{Re}[\varepsilon_3] < 0$) of the film DP ε_3 is negative, while the DPs ε_1 and ε_2 of the separated media are positive real values ($\varepsilon_1, \varepsilon_2 \in \Re$ and $\varepsilon_1, \varepsilon_2 > 0$). This structure maintains the waveguide propagation of SPP in the film with the dispersion.

Parameters determined by both the material characteristics and film thickness. The Cartesian coordinate system is oriented in such a way as to provide SPP propagation along the x axis and the z axis to be perpendicular to the film plane (figure 1).

The dispersion and nonlinear parameters (3)–(6) of SPP waves in a conductive film of a constant h can be calculated using the dispersion relation [16, 17]:

$$\exp(-2q_3h) = \frac{q_3\varepsilon_1 + q_1\varepsilon_3}{q_3\varepsilon_1 - q_1\varepsilon_3}\frac{q_3\varepsilon_2 + q_2\varepsilon_3}{q_3\varepsilon_2 - q_2\varepsilon_3}, \tag{9}$$

where $q_j = \sqrt{\beta^2 - k_0^2\varepsilon_j}$ ($j = 1, 2, 3$) is the component of the wave vector perpendicular to the interfaces, $k_0 = \omega/c$, c is the speed of light in vacuum.

As a conductive film, we assume a material with the DP obtained as:

$$\varepsilon_3 = \varepsilon_\mathrm{L} + \varepsilon_\mathrm{NL}(I), \tag{10}$$

where:

$$\varepsilon_\mathrm{L} = \varepsilon_\infty - \frac{\omega_p^2}{\omega(\omega + i\gamma_e)} \tag{11}$$

is the linear part of the DP recorded using the Drude model, ε_∞ is DP high-frequency component, ω_p is the plasma frequency of electron gas in metal, γ_e is the relaxation rate,

$$\varepsilon_\mathrm{NL} = \alpha I \tag{12}$$

is the nonlinear part that is dependent on the field intensity I, $\alpha \approx 2n_\mathrm{L}n_\mathrm{NL}$, n_L and n_NL are the linear and nonlinear parts of the refractive index $n_3(I) = n_\mathrm{L} + n_\mathrm{NL}I$. The nonlinear DP coefficients can be obtained using the table values of the third-order nonlinear susceptibility $\chi^{(3)}$ [18].

In this study, the numerical simulation has been performed considering silver as a conducting film material. Silver films of thickness of several nanometers in the optical range exhibit the third-order nonlinear susceptibility as high as $\chi^{(3)} \approx 2.5 \times 10^{-8}$ esu [19]. The parameters included in expression (10) in the optical range are $\varepsilon_\infty = 5$, $\omega_\mathrm{p} = 13.5 \times 10^{15}$ s^{-1} [20]. At room temperature, the electron relaxation rate for silver is as high as $\gamma_e \approx 6 \times 10^{13}$ s^{-1} [20] leading to high maximal values of the imaginary part of dielectric constant (11) ($\mathrm{Im}(\beta) > 10^8$ m^{-1}) in a relatively wide frequency range. Under these conditions, within the given frequency range, the SPP free path is estimated to be 10 nm and less. It is not enough to observe drastic changes of the SPP caused by the MI. On the other hand, in this frequency range (corresponding to the highest values of $\mathrm{Im}(\beta)$) the effects associated with the thickness of metal film h are the most pronounced. Therefore, $\gamma_e = 10^{12}$ s^{-1} is used in our calculations to increase the SPP free path by some orders of magnitude. Physically, such γ_e values correspond to silver films cooled down to some low temperatures. High-purity silver samples at liquid helium temperature exhibit $\gamma_e < 10^{12}$ s^{-1} [21].

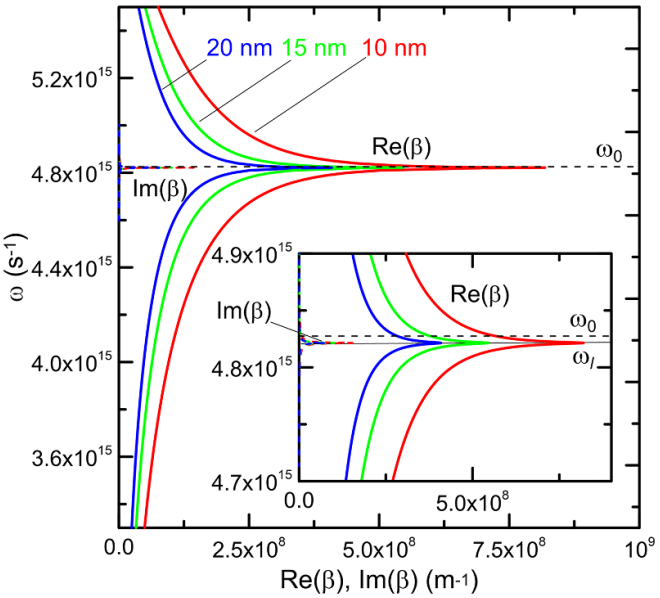

Figure 2. Dispersion curves for SPP modes in the silver film ($h = 10$ nm): (red curve), 15 nm (green curve), 20 nm (orange curve) on dielectric substrate. Solid curves are for Re(β) and dashed are for Im(β). Inset: dispersion curves around the chosen frequency $\omega_0 = 4.823 \times 10^{15}$ s^{-1}.

The dispersion relations for the real and imaginary parts of propagation constant in the linear approximation ($\alpha = 0$) for silver films of various thickness on dielectric Al_2O_3 substrate ($\varepsilon_1 = \varepsilon_2 = 2.84$) are plotted in figure 2. Figure 2 shows that the frequency ω_l corresponding to the maximal β divides the dispersion curves into those describing the upper (high-frequency) and lower (low-frequency) SPP modes. The behavior of dispersion parameters (3)–(6) is different for these modes. Thus, in the considered frequency range, the parameter β_1 (3) inverse to the group velocity v_g is positive on the lower mode but it changes its sign and it is negative on the upper mode. One should note that the negative group velocity is typical for high-frequency plasmon mode in thin metal film [22]. The GVD parameter β_2 (5) is maintained positive for both modes, since the positive value β_1 increases with ω on the lower mode, while on the upper mode an increase of the negative β_1 in the absolute value corresponds to the frequency decrease.

For noble metals, $\alpha > 0$, thus $\frac{\partial\omega}{\partial I}\big|_{\omega_0, I=0}$ is positive on both branches of SPP dispersion relation:

$$\frac{\partial\omega}{\partial I}\big|_{\omega_0, I=0} \approx \alpha\left(\frac{\partial\varepsilon_L}{\partial\omega}\big|_{\omega=\omega_0}\right)^{-1} = \alpha\frac{\omega_0^3}{2\omega_\mathrm{p}^2} > 0. \tag{13}$$

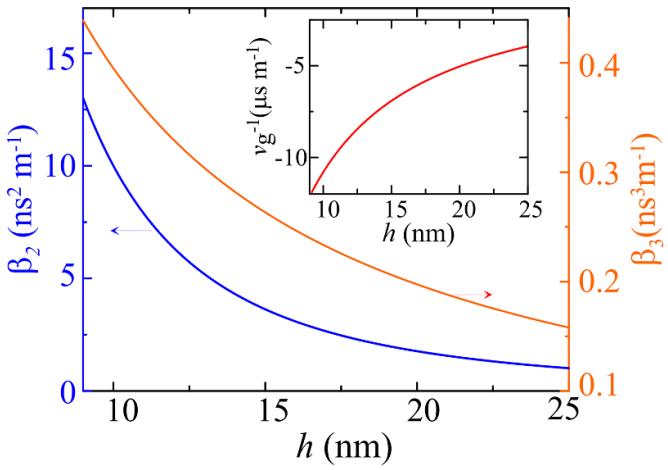

Figure 3. GVD (blue line) and TOD (red line) of the high-frequency dispersion branch as a function of the silver film thickness at $\omega_0 = 4.823 \times 10^{15}$ s^{-1}. The inset shows the same function for the group velocity v_g^{-1} through the length of 10 nm.

Hence, taking into account relation (7), the Kerr nonlinearity parameter γ and SPP group velocity are of the same signs. Therefore, the parameter γ is always positive for the low-frequency SPP mode and negative for the high-frequency SPP mode within some range of β. So, on the upper mode within this range of β the GVD β_2 and Kerr nonlinearity parameter γ of SPP have opposite signs enabling the MI [8]. One should note that the slope angle range of dispersion curves corresponding to different h increases with an approach to the limiting frequency ω_l. Thus, the dispersion parameters (3)–(6) exhibit stronger dependence on the thickness h at $\omega_0 \to \omega_l$. For further calculations we use $\omega_0 = 4.823 \times 10^{15}$ s^{-1} since this value is close to the limiting frequency ω_l but it provides significantly lower absorption: $\mathrm{Im}(\beta(\omega_0)) \approx 0.6 \times 10^7$ m^{-1} << $\mathrm{Im}(\beta(\omega_l)) \simeq 10^8$ m^{-1} (figure 2). The parameter of nonlinearity can be estimated as:

$$\gamma = v_g^{-1}|_{\omega_0, I=0} \frac{\alpha \omega_0^3}{2\omega_p^2} \approx v_g^{-1}|_{\omega_0, I=0} \cdot 245\,\mathrm{m^2W^{-1}\,s^{-1}}. \quad (14)$$

Near $\omega = \omega_0$, the real part of the propagation constant increases with the decreasing film thickness and ranges within 10^8 m^{-1}–7×10^8 m^{-1} for a film with h varying from 9 nm to 25 nm.

The GVD and TOD obtained by numerical differentiation of dispersion relations (9) for $\omega = \omega_0$ as a function of the film thickness h are given in figure 3. The inset shows similar dependence for the inverse group velocity v_g^{-1}. One can see that the SPP wave dispersion parameters exhibit a strong dependence on the film thickness h while the high GVD and TOD values, typical for thin films, decrease quickly with increasing h. Also, with an increase of h, the absolute value of v_g^{-1} and γ proportional to it rapidly decrease.

As mentioned above, around $\omega_0 = 4.823 \times 10^{15}$ s^{-1}, the MI condition $\gamma\beta_2 < 0$ is fulfilled, i.e. for a given frequency domain, any weak time-periodic modulation of the steady-state SPP wave increases with a certain increment dependent on both the wave intensity I and modulation frequency Ω. The modulation gain for weak periodic perturbations is determined by the GVD β_2 and Kerr nonlinearity γ [8, 23]:

$$g_m(\Omega) = |\beta_2 \Omega| \sqrt{\Omega_c^2 - \Omega^2}, \quad (15)$$

where:

$$\Omega_c = 2\sqrt{\left|\frac{\gamma}{\beta_2}\right| I} \quad (16)$$

is the maximal frequency of MI. A strong dependence of the dispersion parameters on the film thickness makes the modulation gain (15) change drastically with h. Figure 4 shows the modulation gain $g_m(\Omega)$ for different thickness of a silver film at the initial intensity of modulated wave $I = 10^{-2}$ W μm^{-2}. One can see that the specific nonlinear and dispersion parameters of the plasmon structure could enable drastically high MI gain that is sufficient to ensure breaking of the modulated wave into individual pulses while it propagates

The maximal modulation gain for thin films ($h \approx 10$ nm) is more than twice as high as that for relatively thick films ($h > 20$ nm). However, thick films have a wider MI frequency range. For this reason, the MI of ultrahigh-frequency ($\Omega > \pm 1.5 \times 10^{13}$ s^{-1}) modulations can be observed only in relatively thick films. Comparing the obtained MI frequency range for different h (figure 4) with the graphs of dispersion ratios (figure 2) one should note that the MI range remains within the upper mode, i.e. does not go beyond the range of negative values of v_g^{-1}. Although the values of dispersion parameters change drastically even with small variations of the frequency ω, the considered approach is still applicable within the entire frequency range available for MI.

4. Modulation instability of SPP waves in a film of constant thickness

Here, we explore the MI in a silver film with a constant thickness in the direction of SPP propagation (see figure 1, $\varepsilon_1 = \varepsilon_2 = 2.84$) codirectional with the x-axis in the Cartesian coordinate system. To describe the evolution of a modulated wave, we use the NLS equation (8) taking into account the absorption determined by the imaginary part of propagation constant,

$$\frac{\partial A}{\partial x} + v_g^{-1}\frac{\partial A}{\partial t} + \frac{i\beta_2}{2}\frac{\partial^2 A}{\partial t^2} - \frac{\beta_3}{6}\frac{\partial^3 A}{\partial t^3} - i\gamma|A|^2 A = -\mathrm{Im}(\beta)A. \quad (17)$$

As the initial conditions, we use a modulated wave $A(t,0) = \sqrt{I_0}(0.99 + 0.01 \cdot \cos(2\pi\nu_m t))$ with the intensity $I_0 = 10^{-2}$ W μm^{-2} at $t = 0$, where $\nu_m = (\omega_0 - \omega_s)/2\pi$ is the modulation frequency, ω_s is the frequency of the second (modulating) component. Frequency modulation can be induced by two sources operating at close wavelengths or generated from a spontaneous noise (spontaneous MI) [8, 24]. For the

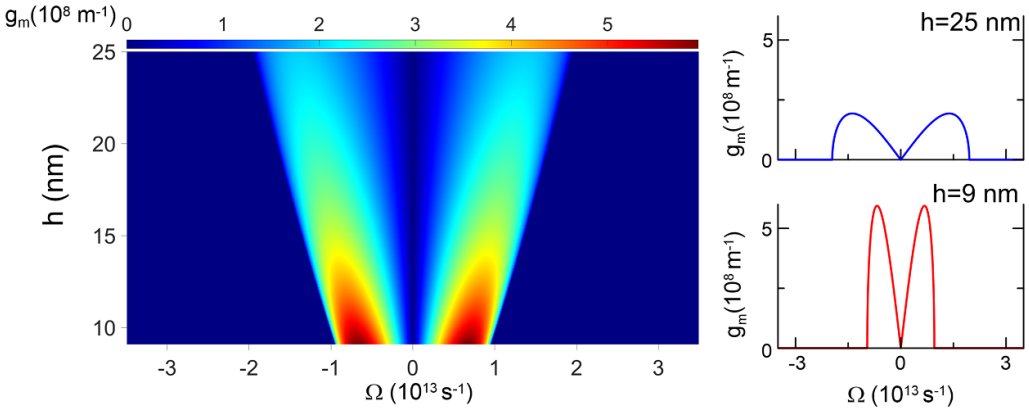

Figure 4. Modulation gain (15) calculated for different film thickness. The initial intensity of modulated wave is $I = 10^{-2}$ W μm^{-2}. Right: modulation gain at $h = 9$ nm and $h = 25$ nm.

numerical modeling of the equation (17) the well-known split-step Fourier method is used. Verification of our simulations was carried out by comparing the obtained numerical results with the results achieved on the grid with double precision. In all our simulations, the difference between the obtained numerical values did not exceed 0.5%. The simulation results describing evolution of the SPP wave for films of the thickness $h = 10$ nm and $h = 20$ nm are shown in figure 5 at the periodic boundary conditions. The modulation frequencies for each film $\nu_m = 1.33$ THz (a), (b) and $\nu_m = 2$ THz (c), (d) are chosen so that the modulation gain shall be close to its possible maximal value corresponding to the given film thickness.

One can see that due to very high modulation gain, the MI process is developing very fast—the modulated wave transforms into a train of contrast subpicosecond pulses after propagation over some tens of nm in the film. The modeling results on the modulation gain show that in a thicker film the pulses are generated more slowly though exhibiting shorter duration due to a wider MI spectrum. In is worth noting that the evolution of modulated SPP wave in the film occurs in a periodic manner—the pulse train generation is cyclically altered by a return to the initial state of modulated wave. Due to absorption, the SPP wave intensity is constantly decreasing.

5. Modulation instability of SPP waves in a film of varying thickness

Let us consider the SPP propagation in the film of varying thickness $h = h(x)$. Schematic of the structure is given in figure 6. In the direction of the y-axis, the parameters of structure and SPP are invariable. Thus, we focus on the fields in the xz plane only. The media material parameters are the same as given above.

With a smoothly varying film thickness, the dispersion and nonlinear parameters (3)–(6) can be determined in the adiabatic approximation: the local values of these parameters at the points with a coordinate $x = x_0$ can be determined from the analytical expressions obtained for a film of constant thickness $h(x_0)$. Quasi-adiabatic approximation can be applied if the following inequality is fulfilled:

$$\left|\frac{\beta(h_2) - \beta(h_1)}{\beta(h_1)}\right| << 1, \tag{18}$$

where $\beta(h)$ is the propagation constant of SPP in a film of local thickness $h = h(x)$, $|h_2 - h_1| \geqslant 2\pi/\mathrm{Re}(\beta)$. When this inequality and relations (3)–(6) are fulfilled, the local values of the SPP parameters in a film of variable thickness can be calculated using the mathematical apparatus of the previous section applied for a film of constant thickness.

The considered mechanism is similar to the MI in a waveguide with the parameters varying along its length. The SPP propagation in a film of constant thickness discussed in section 4 can be considered as a particular case of radiation propagation in a waveguide with the parameters constant along the length, while the MI process is repeatable. Meanwhile, in the spectral domain, the spectrum exhibits periodically repeated behavior. The spectrum of a continuous wave with two initial harmonics corresponding to the modulation frequency $\pm\Omega_m$ transforms into a wide spectrum corresponding to a pulse train and then returns back to the initial state and so on [8, 24].

It is known that in a waveguide with a GVD varying along the length, the bandwidth of MI gain spectrum $(-\Omega_c, \Omega_c)$ and the peak frequency of MI gain spectrum $\Omega_{\max} = \Omega_c \Big/ \sqrt{2}$ increase along the waveguide length as GVD decreases [25, 26]. With the wave propagation in direction of the decreasing GVD the cyclicity of transformation of the pulse train into the weakly modulated wave and back is violated. An increase of the MI bandwidth involves larger number of high-frequency spectral components in the process, thus shortening the duration of the generated pulses. As a result, the process of MI becomes irreversible enabling effective generation of high-repetition ultrashort pulse trains. The calculation of the MI gain for films of different thickness (see figure 4) shows that a similar process can be observed for a modulated SPP wave propagating in a metal film of varying thickness. In this case, to obtain a waveguide with a decreasing GVD, SPP

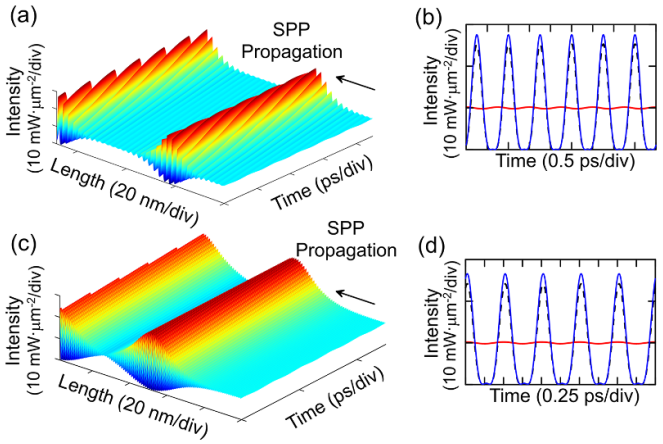

Figure 5. Modulation instability of SPP in Ag film of different thickness h: $h = 10$ nm, modulation frequency $\nu_m = 1.33$ THz (a), (b); $h = 20$ nm, $\nu_m = 2$ THz (c), (d). Evolution of SPP intensity (a), (c); initial SPP intensity (red) and SPP intensity after propagation of 22 nm (blue), 67 nm (dashed) (b); of 43 nm (blue), 96 nm (dashed) length (d).

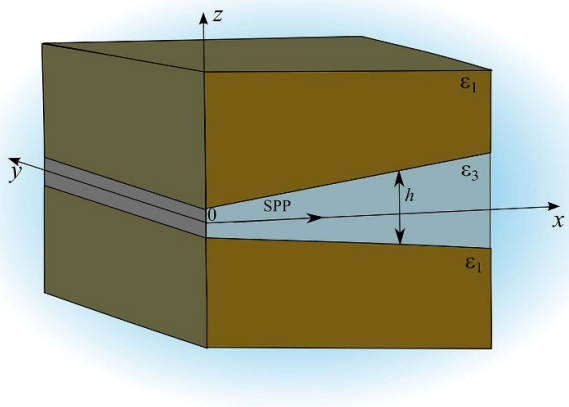

Figure 6. Structure of a planar metal film of varying thickness: metal film (ε_3) with linearly varying thickness $h(x)$ separates the dielectric media with the same DP ε_1.

has to propagate in such a way that the film thickness increases in the direction of its propagation.

To simulate the SPP wave propagation one can use equation (17) taking into account the change of SPP mode area along the length:

$$\frac{\partial A}{\partial x} + \nu_g^{-1}(x)\frac{\partial A}{\partial t} + \frac{i\beta_2(x)}{2}\frac{\partial^2 A}{\partial t^2} - \frac{\beta_3(x)}{6}\frac{\partial^3 A}{\partial t^3} - i\gamma(x)|A|^2 A = \left(Im(\beta) + \frac{1}{2S_m(x)}\frac{\partial S_m(x)}{\partial x}\right)A, \tag{19}$$

where $S_m = \int_{-\infty}^{\infty}\int_{-\infty}^{\infty}(U(y,z)/U(y=0,z=0))\mathrm{d}z\mathrm{d}y$ is the mode area of plasmonic waveguide. In contrast to equations (8) and (17), the coefficients in (19) are the functions of the x coordinate, i.e. they change along the direction of SPP propagation. The change of plasmon mode area $S_m(x)$ along the direction of SPP propagation can be determined using the known relations for the SPP field distribution in a conductive film [27].

For simulation, we use the same initial conditions and carrier frequency ω_0 as in section 4 and the frequency modulation $\nu_m = 0.89$ THz. Figures 7(a) and (b) show the distribution of nonlinear and dispersion coefficients along the coordinate x with the film thickness linearly increasing from 9 nm with the rate of about 1.6 nm per 10 nm film length. The film thickness is shown by a black curve in figure 7(a). Figure 7(b) illustrates also evolution of the SPP peak intensity during propagation. Figure 7(c) shows the evolution of intensity $I = |A|^2$ for SPP wave. The intensities of initial modulated wave and SPP wave propagating over ~67 nm in a film with a linearly increasing thickness are compared in figure 7(d). The above dependences show that the intensity of SPP wave is modulated in space and time and almost sevenfold increase of the SPP wave peak intensity is recorded after the propagation over ~67 nm. The SPP path length l calculated from $l \simeq 1/\mathrm{Im}(\beta) \approx 167$ nm, thus, the effective transformation of SPP induced by MI is observed at relatively short distances and attenuation does not significantly affect the MI effect (see figure 7(c)). TOD and variation of the group velocity parameter υ_g^{-1} along the length break the shape symmetry of the generated pulse. However, a high modulation gain in combination with the spectrum constantly broadening along the length ensures their ultrashort duration ($\tau < 100$ fs).

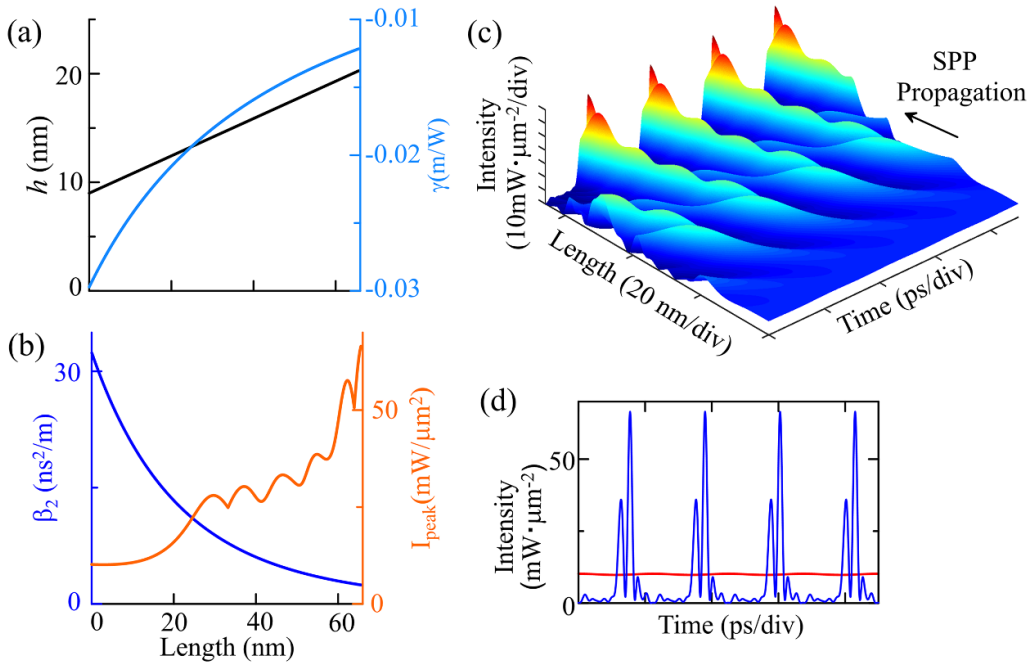

Figure 7. (a) Film thickness and Kerr nonlinearity coefficient (7) as a function of the SPP propagation length. (b) Group velocity dispersion and peak intensity of the SPP wave as a function of the SPP propagation length. (c) Evolution of the SPP intensity in a film with linearly increasing thickness by 1.6 nm per 10 nm length. The initial SPP wave intensity is $I_0 = 10^{-2}$ W μm^{-2}, the modulation frequency is $\nu_m = 0.89$ THz.

6. Conclusions

SPP wave propagating in dielectric—thin metal film-dielectric structure has been considered. Using standard approximations, we have derived the NLSE propagation equation taking into account the Kerr phase shift of propagating SPP wave. Based on the dispersion relation, the SPP dispersion and nonlinear characteristics are obtained as well as their dependences on metal film thickness. It is shown that the dispersion and nonlinear properties of thin-film plasmonic structures can provide a very high modulation gain leading to conversion of a modulated SPP wave into an ultrashort pulse train while propagating over a few 10 nm.

Propagation and transformation of an intense modulated SPP wave in a silver film of constant and increasing thickness have been simulated. We have determined the structure parameters enabling MI in SPP leading to generation of subpicosecond pulses with a terahertz repetition rate. It is shown that the modulated SPP wave transforms into a THz train of ultrashort pulses within a very short propagation length of some 10 nm.

The proposed concept is greatly promising for development of compact generators of high repetition rate (∼1 THz) ultrashort (∼100 fs) pulse trains and applicable for multiple tasks of modern optoelectronics, including development of master clocks, frequency comb generators, and etc. The obtained results can be employed to implement the self-induced transparency regime in a metal, as predicted in [28, 29]. This technique opens up prospects for further advancement of plasmonic technologies providing compensation of high ohmic losses for strongly confined SPPs.

Data availability statement

All data that support the findings of this study are included within the article (and any supplementary files).

Funding

This work was supported by the Ministry of Higher Education and Science of the Russian Federation (Project #075-15-2021-581) and the Russian Foundation for Basic Research (Grants #18-29-19101, #19-42-730010, #18-42-730007).

Conflict of interest

The authors declare no conflicts of interest.

ORCID iDs

Dmitry A Korobko https://orcid.org/0000-0002-1582-7567
Igor O Zolotovskii https://orcid.org/0000-0002-1793-5211
Sergey G Moiseev https://orcid.org/0000-0001-8252-7997

References

[1] Zayats A V, Smolyaninov I I and Maradudin A A 2005 Nano-optics of surface plasmon polaritons *Phys. Rep.* **408** 131–314
[2] Kauranen M and Zayats A 2012 Nonlinear plasmonics *Nat. Photon.* **6** 737–48

[3] Zia R, Schuller J A, Chandran A and Brongersma M L 2006 Plasmonics: the next chip-scale technology *Mater. Today* **9** 20–27
[4] Fang Y and Sun M 2015 Nanoplasmonic waveguides: towards applications in integrated nanophotonic circuits *Light Sci. Appl.* **4** e294
[5] Zolotovskii I O, Dadoenkova Y S, Moiseev S G, Kadochkin A S, Svetukhin V V and Fotiadi A A 2018 Plasmon-polariton distributed-feedback laser pumped by a fast drift current in graphene *Phys. Rev.* A **97** 053828
[6] Morgado T A and Silveirinha M G 2021 Active graphene plasmonics with a drift-current bias *ACS Photonics* **8** 1129–36
[7] Scott A C 2007 *The Nonlinear Universe: Chaos, Emergence, Life* (Berlin: Springer)
[8] Agrawal G P 2013 *Nonlinear Fiber Optics* (NY: Academic)
[9] Lugiato L A and Lefever R 1987 Spatial dissipative structures in passive optical systems *Phys. Rev. Lett.* **58** 2209–11
[10] Clerc M G, González-Cortés G and Wilson M 2016 Extreme events induced by spatiotemporal chaos in experimental optical patterns *Opt. Lett.* **41** 2711–4
[11] Zolotovskii I O, Korobko D A and Lapin V A 2014 Modulation instability and short-pulse generation in media with relaxing Kerr nonlinearity and high self-steepening *Quantum Electron.* **44** 42–48
[12] Tajima K 1986 Self-amplitude modulation in PSK coherent optical transmission systems *J. Lightwave Technol.* **4** 900–4
[13] Mamyshev P V, Chernikov S V, Dianov E M and Prokhorov A M 1990 Generation of a high repetition-rate train of practically noninteracting solitons by using the induced modulational instability and Raman self-scattering effects *Opt. Lett.* **15** 1365–7
[14] Närhi M, Wetzel B, Billet C, Toenger S, Sylvestre T, Merolla J-M, Morandotti R, Dias F, Genty G and Dudley J M 2016 Real-time measurements of spontaneous breathers and rogue wave events in optical fibre modulation instability *Nat. Commun.* **7** 1–9
[15] Swanson E A and Chinn S R 1994 23 GHz and 123 GHz soliton pulse generation using two CW lasers and standard single-mode fiber *IEEE Photonics Technol. Lett.* **6** 796
[16] Economou E N 1969 Surface plasmons in thin films *Phys. Rev.* **182** 539
[17] Maier S A 2007 *Plasmonics: Fundamentals and Applications* (Berlin: Springer) p 221
[18] Boyd W 2008 *Nonlinear Optics* (Amsterdam: Elsevier) p 610
[19] Yang G, Guan D, Wang W, Wu W and Chen Z 2004 The inherent optical nonlinearities of thin silver films *Opt. Mater.* **25** 439–43
[20] Yang H U, d'Archangel J, Sundheimer M L, Tucker E, Boreman G D and Raschke M B 2015 Optical dielectric function of silver *Phys. Rev.* B **91** 235137
[21] Kittel C 2005 *Introduction to Solid State Physics* (NY: Wiley)
[22] Fedyanin D, Arsenin A V, Leiman V G and Gladun A D 2009 Surface plasmon—polaritons with negative and zero group velocities propagating in thin metal films *Quantum Electron.* **39** 745–50
[23] Moiseev S G, Korobko D A, Zolotovskii I O and Fotiadi A A 2017 Evolution of surface plasmon–polariton wave in a thin metal film: the modulation-instability effect *Ann. Phys.* **529** 1600167
[24] Erkintalo M, Hammani K, Kibler B, Finot C, Akhmediev N, Dudley J M and Genty G 2011 Higher-order modulation instability in nonlinear fiber optics *Phys. Rev. Lett.* **107** 253901
[25] Chernikov S V, Dianov E M, Richardson D J, Laming R I and Payne D N 1993 114 Gbit/s soliton train generation through Raman self-scattering of a dual frequency beat signal in dispersion decreasing optical fiber *Appl. Phys. Lett.* **63** 293–5
[26] Panyaev I S *et al* 2021 High-frequency pulse train generation in dispersion-decreasing fibre: using experimental data for the metrology of longitudinally nonuniform fibre *Quantum Electron.* **51** 427–33
[27] Agranovich V M and Mills D L (eds) 1982 *Surface Polaritons* (North-Holland, Amsterdam: Elsevier)
[28] Belenov È M and Kanavin A P 1993 Propagation of ultrashort light pulses in metals *Quantum Electron.* **23** 335–6
[29] Belenov È M *et al* 1993 Electrodynamics of the propagation of ultrashort light pulses in metals *JETP Lett.* **58** 333–7